Analysis and Parametric Optimization of a Turn of a Meander Line with Broad-Side Coupling in Different Environments

Konstantin Malygin[a)], Alexander Nosov[b)] and Roman Surovtsev[c)]

Department of Television and Control Tomsk State University of Control Systems and Radioelectronics, Tomsk, Russia

[a)] Corresponding author: malyginkp@gmail.com
[b)] alexns2094@gmail.com
[c)] surovtsevrs@gmail.com

Abstract. The paper presents the results of the analysis and parametric optimization of a meander line with a broad-side coupling in different climatic conditions. The optimization was performed by the two methods: genetic algorithms (GA) and evolutionary strategies (ES), and using one and two criteria. Different environmental conditions were represented by ice, water and air. The analysis showed that changing from the air filling layer to the water layer increased the per-unit-length delays of the even and odd modes by 39% and 12%, and introducing the ice layer – by 177% and 248%, respectively. The optimization results of the two methods showed good agreement. However, with the obtained similar sets of optimal parameters, the optimization using ES was up to 3.3 times faster than the optimization using GA.

INTRODUCTION

Radio-electronic equipment (REE) has long been actively used in many industries including military and aerospace. Such equipment operates in particularly difficult and often inclement climatic conditions that can negatively affect its specified characteristics. First of all, in the near-Earth orbit, metal under direct sunlight heats up to 160°C, and in the shade, it cools down to minus 100°C. Second, a change of the ambient temperature can lead to a change in the chemical-physical and mechanical properties of materials [1]. With an increase in temperature, the evolvement of material defects is accelerated, which leads to a decrease in the strength of joints and structural elements. In addition, under the simultaneous influence of temperature and physical stress, most materials are subject to deformation. For a number of materials, heating causes chemical decomposition and accelerated aging. Third, the characteristics of the REE can also be affected by the processes happening in water when the temperature changes. The temperature change leads to the changes in air humidity, which results in dew; and at a negative temperature, the water passes into a solid state. Therefore, depending on the field of REE application, testing REE also includes climatic tests [2]. Meanwhile, full-scale tests and retests in case of their negative results can be very costly. Therefore, taking into account climatic factors at an early design stage will minimize these costs, which urges the preliminary simulation and optimization.

One of the important aspects in the REE design is to ensure its uninterrupted operation under the influence of electromagnetic interference (EMI). This aspect is especially important for REE in the aerospace industry because of the complex electromagnetic environment of the orbit. Continuous improvement of REE (reduction of operating voltages and increase in the upper frequencies of the signals spectrum used) results in an increase in the sensitivity of its elements to EMI that can be both natural (electrostatic discharge, secondary lightning effects) and intentional (IEMI) [3]. Pulses of the nanosecond and subnanosecond ranges (or ultrashort pulses, USPs) are of particular danger to REE [4]. The most well-known means of protection against such pulses are interference suppressors, electromagnetic shields, decoupling devices, various filters, and gas dischargers. There are also devices based on printed structures for interference suppression and signal filtering in the frequency band [5–10]. However, traditional solutions have a number of disadvantages that make it difficult to use them in critical REE. These disadvantages

include low power and speed [11], parasitic effects [12], and loss of properties of the insulating dielectric between the capacitor plates [13].

A noteworthy approach to the REE protection is based on the use of distortions in printed structures – meander lines (ML) [14, 15]. Its advantage is that its implementation may not require a protection device as such, but employ the MLs that are already on the PCB. The approach is based on the decomposition of a USP into a sequence of pulses of smaller amplitudes by optimizing the parameters of the structure cross-section. Another similar approach is the USP decomposition in coupled lines (modal filters) [16, 17]. However, in the simplest case, with the same lengths and cross-section parameters, an ML turn allows for a greater attenuation by decomposing the pulse (moreover with doubled duration) into a larger number of pulses. Meanwhile, the use of such protection technique in practice in difficult climatic conditions requires their preliminary detailed simulation in the temperature range and optimization of their parameters, taking into account the influence of various climatic conditions. In paper [18], the optimization took into account the change in the ambient temperature from minus 50 to 150 degrees Celsius. However, the effect of water and ice properties on these structures has not been studied. Heuristic search optimization will require a significant amount of time and may not lead to an acceptable result. Therefore, it seems necessary to use global optimization methods (genetic algorithms (GA) and evolutionary strategies (ES)), since they are quite easy and implemented in the TALGAT software available for the authors of this paper [19]. Thus, the purpose of this work is to analyse the influence of water and ice on the characteristics of a simple structure (a turn of an ML with a broad-side coupling [15]) and demonstrate the possibility of optimizing its parameters taking into account the influence of water and ice.

TEMPERATURE MODEL

When simulating ice, it is assumed that the temperature is negative. Therefore, further simulation will take into account the influence of temperature. For simulation, we chose a temperature model that was previously tested on a single microstrip line [20]. The temperature model has the general view $P(T)$ where P is one of the structural characteristics, T is the current ambient temperature. The temperature model of each line parameter is implemented according to the known expression

$$x = x_o\left(1+\alpha\Delta T\right), \tag{1}$$

where x is the value of the line parameter that takes into account thermal expansion, x_0 is the initial value of this parameter, α is the coefficient of linear thermal expansion of the material, and ΔT is the temperature difference. The value of α for copper is assumed to be $17\cdot10^{-6}$ in accordance with [21], and for the dielectric substrate (FR-4 material) along the Z axis it is $70\cdot10^{-6}$, and along the X and Y axes it is $17\cdot10^{-6}$ [22].

The temperature dependence of electrophysical parameters can be considered in a similar way. For relative permittivity (ε_r), the FR-4 coefficient α was obtained based on data from [23] as

$$\alpha = \frac{\varepsilon_{r\,max}-\varepsilon_{r\,min}}{T_{max}-T_{min}} = -55\cdot10^{-4}\cdot\mathrm{K}^{-1} \tag{2}$$

where T_{max} and $T_{\min}$ are the maximum and minimum values of the temperature range, and $\varepsilon_{r\,max}$ and $\varepsilon_{r\,min}$ are the maximum and minimum values of ε_r for the extreme points of the T range.

INITIAL DATA

The cross-section of the ML turn with a broad-side coupling under investigation is shown in Fig. 1a. Its parameters are the following: d is the distance from the edge of the structure to the conductor ($3w$), w is the width of the conductors (6000 μm), s is the distance between the conductors (200 μm), t is the thickness of the conductors (18 μm), h is the distance between the grounded and signal conductors (2100 μm), and ε_r is the permittivity of the substrate (4.4). The circuit diagram of the turn is shown in Fig. 1b. As an excitation, we used a USP with an e.m.f. amplitude of 1 V and a flat top duration of 100 ps, and a rise and fall time durations of 50 ps each. The length of the half-turn (l) is 30 mm. These geometric parameters of the ML with broad-side coupling will be called later as initial.

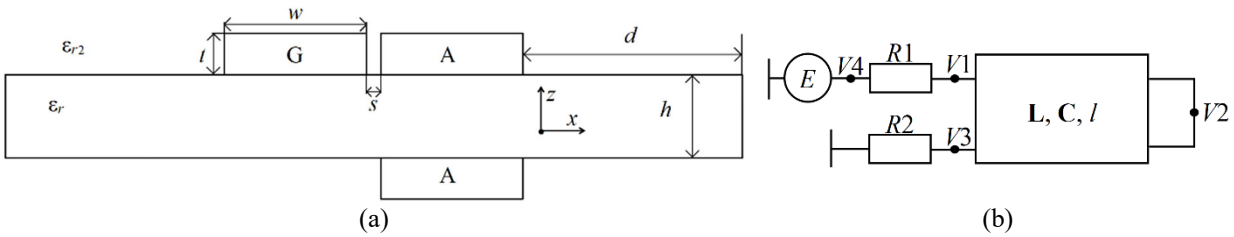

FIGURE 1. Cross section (a) and circuit diagram (b) of the ML turn with broad-side coupling.

ANALYSIS OF CHANGES IN THE TURN PARAMETERS WITH CHANGES IN THE ENVIRONMENT

During simulations, the environment changed: a layer of water (ε_{r2}=81) or ice (ε_{r2}=4) 1 mm thick was assumed to be introduced along the surface of the line. For water it was assumed that T=25°C, and for ice – T=–50°C. Table 1 summarizes the calculated relationships between the per-unit-length delays of even (τ_e) and odd (τ_o) modes, their impedances Z_e and Z_o, and the output voltage amplitudes (U_{max}) of the turn and T, using the initial parameters.

TABLE 1. Relationships between τ_e, τ_o, Z_o, Z_e and U_{max} and the environment.

Layer	τ_e, ns/m	τ_o, ns/m	Z_e, Ohm	Z_o, Ohm	U_{max}, V
Ice (ε_{r2}=4, T=–50°C)	6.86	7.06	19.90	92.64	0.332
Water (ε_{r2}=81, T=25°C)	21.95	13.64	9.40	31.69	0.188
Air (ε_{r2}=1, T=25°C)	4.92	6.31	22.59	127.69	0.206

Table 1 shows that in the presence of a water layer, the values of per-unit-length delays of even and odd mode pulses and their differences significantly increase. It should also be noted that in this case the fast and the slow mode delays are reversed ($\tau_e > \tau_o$). In the presence of an ice layer, their values also increase, but their difference decreases. The Z_o and Z_e values for the turn in the ice layer decrease by 2.68 Ohm and 35.04 Ohm, respectively, and in the water layer by 13.18 Ohm and 95.99 Ohm, respectively. Fig. 2 shows a simulation model of the time response at the output of the structure covered by ice, water, and air.

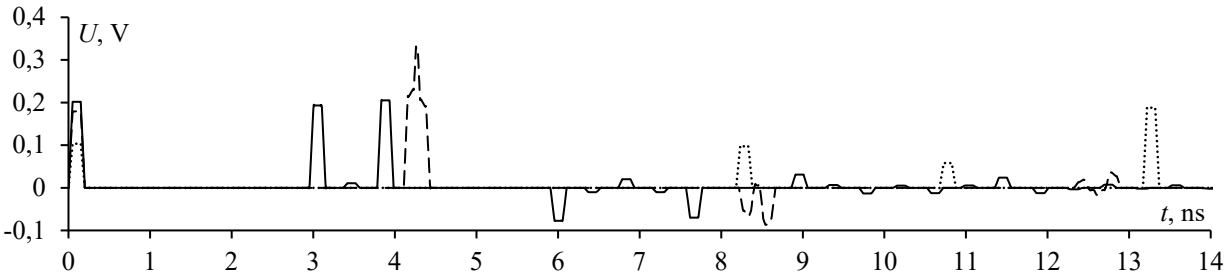

FIGURE 2. Time responses at the output of the turn covered by ice (– –), water (• • •), and air (—).

The time responses illustrate that the maximum voltage values at the end of the turn are different for various conditions: 0.3315 V for the ice layer, 0.18847 V for the water layer, and 0.20598 V in the air filling. This difference in amplitudes was due to the superposition of even and odd mode pulses on each other in the ice-covered line. The minimum amplitude value at the line output was obtained for the water-covered line. Thus, the water layer in the structure contributes to improving its protective characteristics by minimizing the amplitude at its output. The delays of the first and second pulses for the ice-covered turn (compared with the air filling case) increased by 39.3% and 12%, respectively. Meanwhile, when the turn is covered by the water layer, they increased by 177.1% and 248%, respectively.

Then, we analysed the influence of geometric parameters on τ_e, τ_o, Z_o, Z_e, and U_{max} in the air filling and covered by water and ice layers. The obtained results with changes of the turn parameters (s, h and ε_r) are summarized in Tables

2–4. Note that when any parameter of the structure changes, the other parameters are fixed and taken as initial ones. Also note that when changing ε_r, coefficient α corresponds to the material FR-4 and was calculated by expression (2).

TABLE 2. Relationship between τ_e, τ_o, Z_o, Z_e and U_{max} and s.

s, μm	Layer	τ_e, ns/m	τ_o, ns/m	Z_e, Ohm	Z_o, Ohm	U_{max}, V
100	Ice	6.8574	7.0621	19.306	83.771	0.337
	Water	22.1	13.644	8.8026	29.484	0.1726
	Air	4.9264	6.29	22.076	114.685	0.2012
300	Ice	6.8538	7.0646	20.199	98.927	0.3199
	Water	21.9355	13.6233	9.724	33.25	0.1982
	Air	4.9011	6.3134	22.847	137.248	0.2098
500	Ice	6.84734	7.06579	20.515	108.544	0.29693
	Water	22.0015	13.5914	10.098	35.621	0.20932
	Air	4.85308	6.32055	23.118	152.355	0.21778

TABLE 3. Relationship between τ_e, τ_o, Z_o, Z_e and U_{max} and h.

h, μm	Layer	τ_e, ns/m	τ_o, ns/m	Z_e, Ohm	Z_o, Ohm	U_{max}, V
500	Ice	6.7833	7.1243	6.3488	92.155	0.2678
	Water	19.877	9.6563	4.391	33.663	0.2028
	Air	4.3752	6.6954	6.7849	142.75	0.3106
1000	Ice	6.8195	7.0981	11.4625	91.2740	0.2308
	Water	21.093	11.2874	6.6676	31.9635	0.1945
	Air	4.6517	6.5307	12.5381	133.388	0.2632
1500	Ice	6.8402	7.0797	15.6987	91.5978	0.2538
	Water	21.6128	12.4922	8.159	31.6237	0.191
	Air	4.8031	6.4126	17.4936	129.6320	0.2304

TABLE 4. Relationship between τ_e, τ_o, Z_o, Z_e and U_{max} and ε_r.

ε_r	Layer	τ_e, ns/m	τ_o, ns/m	Z_e, Ohm	Z_o, Ohm	U_{max}, V
6	Ice	7.3044	7.9731	17.6917	86.6552	0.2215
	Water	21.3276	14.3003	9.0371	32.2931	0.1817
	Air	5.4979	7.2902	19.5662	114.177	0.2053
10	Ice	8.2988	9.8679	14.3556	75.9473	0.2306
	Water	32.1574	15.4224	8.505	20.9428	0.1942
	Air	6.7145	9.3003	15.3581	93.3609	0.2207
14	Ice	9.1714	11.4434	12.4039	68.5849	0.2352
	Water	26.0164	17.0654	7.8753	25.6050	0.2029
	Air	7.7359	10.9460	13.0569	80.9857	0.2299

Tables 2–4 shows that increasing the value of s leads to an increase in the difference of τ_o and τ_e of the ice-covered and air-filled lines; however, with the water layer, at s=300 μm, the difference first decreases and then, at s=500 μm, it increases. The values of Z_o and Z_e increase for all cases as the value of s increases. In the ice-covered turn, the U_{max} value decreases with increasing s, and in the water-covered and air-filled turns, it increases. Increasing the value of h leads to an increase in the difference between τ_o and τ_e for all cases. In addition, increasing the h value leads to an increase in the Z_o value, while Z_e decreases. Increasing the value of h in the ice-covered turn, the U_{max} value first decreases and then slightly increases, and in the water-covered and air-filled turns, it decreases. Increase of the ε_r value leads to an increase in the difference of τ_o and τ_e in the ice-covered and air-filled turns. At the same time, in the water-covered turn, the increase of ε_r up to 10 leads first to an increase in the difference of τ_o and τ_e, and then to its decrease at ε_r=14. The U_{max} value for all cases increases when ε_r increases. Thus, we can observe the regularities in how

geometrical parameters influence the characteristics of turns covered by ice, water and in the air filling. These regularities can be used to find the optimal geometric parameters of the turn.

It is also important to note that the maximum changes in the values of τ_o, τ_e, Z_e, Z_o and U_{max} in their variable range differ in the three cases (water, ice, and air filling). To demonstrate this, Table 5 summarizes the maximum deviations of these characteristics for the ranges of s, h and ε_r from Tables 2, 3 and 4. Note that in Table 5 minus and plus signs are introduced to indicate a decrease and an increase in the characteristics, respectively.

TABLE 5. Maximum deviations (%) of τ_e, τ_o, Z_o, Z_e and U_{max} for the entire range of their change for three environments (ice, water, air).

Range	s: 100–300 μm			h: 500–1500 μm			ε_r: 6–14		
Characteristics	Ice	Water	Air	Ice	Water	Air	Ice	Water	Air
τ_e, ns/m	–0.15	–0.39	–1.51	+0.84	+29.37	+9.78	+25.56	+19.34	+40.71
τ_o, ns/m	+0.05	–0.45	+0.49	–0.63	+8.74	–4.41	+43.52	+21.98	+50.15
Z_e, Ω	+6.26	+14.71	+4.72	+147.3	+85.81	+157.8	–42.63	–14.75	–49.85
Z_o, Ω	+29.6	+20.82	+32.85	–0.61	–6.45	–10.12	–26.35	–26.12	–40.98
U_{max}, V	–13.65	+21.3	+8.26	–5.51	–6.2	–34.78	+6.18	+11.7	+11.98

PARAMETRIC OPTIMIZATION OF THE MEANDER LINE WITH BROAD-SIDE COUPLING USING GA AND ES

The parametric optimization of the ML with broad-side coupling using the GA was performed taking into account the temperature model. In the process of optimization, the width of the conductors (w) and the relative permittivity (ε_r) of the substrate were chosen as the variable parameters. The other geometric parameters remained the initial values. When formulating a multicriteria quality function, it is necessary to bring individual criteria to one of the minimization or maximization tasks. For definiteness, we will further consider the minimization of the sum:

$$F = \sum_i F_i \tag{3}$$

where

$$F_i = M_i \frac{f_i}{K_i} \tag{4}$$

where, for the i-th criterion, f_i is the quality function; K_i is the normalization coefficient; M_i is the weight coefficient; i=0, 1, 2, …, N_C, where N_C is the number of optimization criteria. Coefficient K_i was chosen equal to the maximum possible value of the i-th quality function so that the value of f_i/K_i became dimensionless and took values from 0 to 1 during optimization. Coefficient M_i specifies the significance of the i-th criterion. If the criteria are equivalent, then these coefficients are the same and can be 1 or

$$M_i = \frac{1}{N_C} \tag{5}$$

The first criterion in optimizing the structure using GA is the matching criterion. This criterion is necessary to apply to minimize reflections at the ends of the line. Thus, the well-known condition for matching two coupled lines with resistances R at their ends is defined as the geometric mean of the wave impedances of the even and odd line modes (Z) [24]. However, since the structure is asymmetric, it is impossible to use $R1$=$R2$=Z=50 Ω. Thus, the matching criterion is as follows:

$$f_1 = 0{,}5 - U1,\ K_1 = U1_{max} \tag{6}$$

where $U1$ is the amplitude of the signal at the input of the line, and $U1_{max}$ is the maximum possible value of $U1$. For multicriteria optimization, the weight coefficients (M_1, M_2) of each criterion were taken equal to 0.5 each, and $U1_{max}$ was found as a result of simulation for the extreme values of the variable parameters w and ε_r 300≤w≤600 μm and 2≤ε_r≤8 for ice, 50≤w≤150 μm and 2≤ε_r≤8 for water, 500≤w≤900 μm and 2≤ε_r≤8 for air.

The second important optimization criterion is amplitude minimization. To protect against USPs, the waveform $U(t)$ should be analyzed at the ML output. If the maximum level of $U(t)$ represents the danger, then the expressions for f_i and K_i can be formulated as:

$$f_2 = \max\left|U(t)\right|,\ K_2 = \max\left|E(t)\right| \tag{7}$$

where $E(t)$ is the e.m.f. source.

Then the multicriteria optimization problem is written as a quality function

$$F = M_1 \frac{f_1}{K_1} + M_2 \frac{f_2}{K_2}$$

where K_{1max} and K_{2max} are normalization coefficients that are equal to the maximum values of f_1 and f_2, respectively. The weight coefficients (M_1 and M_2) of each criterion were taken equal to 0.5. The numbers of individuals and generations in GA were taken as 10 and 20, respectively. Such number of calculations for the structure under investigation, when the variable parameters and their ranges are taken into account, allow for the desired set of parameters and good convergence of the values of the required characteristics (the maximum deviations of the obtained values $U1$ and U_{max} are not more than 0.18% and 1.89%, respectively). The average time for one run was about 300 s. First, the optimization was performed only according to the matching criterion. In this case, the invariable geometrical parameters of the ice-covered turn were s=100 μm, t=18 μm, h=200 μm, d=3w, l=0.7 m, for the water-covered turn – s=700 μm, t=10 μm, h=500 μm, d=3w, l=0.1 m, and for the air-filled turn – s=30 μm, t=18 μm, h=400 μm, d=3w, l=0.7 m. The value of U_{max} was found as a result of simulation for the extreme values of the variable parameters w and ε_r and was 0.5714 V for the ice-covered turn, 0.5276 V for the water-covered turn, and 0.58 V for the air-filled turn. The optimization results are presented in Tables 6–8.

TABLE 6. GA Results for the ice-covered turn according to criterion (6).

Launch number	w, μm	ε_r	Z_o, Ω	Z_e, Ω	$U1$, V	U_{max}, V
1	316.5	7.4	24.8	119	0.5	0.208793
2	551.8	3.1	23.5	125.8	0.49979	0.209424
3	412.9	5.1	24	122.8	0.49997	0.209171
4	478.8	4	23.7	124.5	0.49999	0.328459
5	323.5	7.2	24.7	119.5	0.50026	0.207883
				Maximum deviation	0.05%	22.84%

TABLE 7. GA Results for the water-covered turn according to criterion (6).

Launch number	w, μm	ε_r	Z_o, Ω	Z_e, Ω	$U1$, V	U_{max}, V
1	86.1	5	29.8	96.4	0.50005	0.185524
2	92.4	2.5	30.1	96.7	0.50016	0.183406
3	79.8	7.7	29.5	96.2	0.50002	0.188348
4	84.5	5.6	29.7	96.4	0.50015	0.186653
5	85.7	5.2	29.7	96.3	0.49997	0.186452
				Maximum deviation	0.02%	1.33%

TABLE 8. GA Results for the air-filled turn according to criterion (6).

Launch number	w, μm	ε_r	Z_o, Ω	Z_e, Ω	$U1$, V	U_{max}, V
1	892.2	3.4	29	127.9	0.49979	0.20823
2	769.8	3.9	30.3	125.5	0.50037	0.20603
3	573.7	4.9	32.7	121	0.50019	0.196642
4	545.5	5	33.3	120.8	0.50099	0.193622
5	785.5	3.8	30.2	125.9	0.50046	0.20669
				Maximum deviation	0.1%	0.8%

Then, we performed the optimization only according to the criterion of minimizing the amplitude at the ML output. Tables 9–11 summarize its results.

TABLE 9. GA Results for the ice-covered turn according to criterion (7).

Launch number	w, μm	ε_r	Z_o, Ω	Z_e, Ω	$U1$, V	U_{max}, V
1	350.2	2	22	120	0.48463	0.19961
2	332.9	2.3	21.8	119.3	0.48351	0.19953
3	336.1	2.2	22	119.8	0.4847	0.2002
4	331.4	2.3	21.8	119.3	0.48351	0.19952
5	336.1	2.2	21.9	119.7	0.4843	0.19907
				Maximum deviation	0.12%	0.28%

TABLE 10. GA Results for the water-covered turn according to criterion (7).

Launch number	w, μm	ε_r	Z_o, Ω	Z_e, Ω	$U1$, V	U_{max}, V
1	404.71	2.05	15.35	49.3	0.3252	0.17371
2	402.35	2	15.4	49.4	0.3265	0.17402
3	415.29	2.38	15.08	48.75	0.32349	0.17501
4	405.88	2	15.35	49.32	0.32684	0.17447
5	401.18	2.07	15.38	49.36	0.32702	0.17452
				Maximum deviation	0.54%	0.37%

TABLE 11. GA Results for the air-filled turn according to criterion (7).

Launch number	w, μm	ε_r	Z_o, Ω	Z_e, Ω	$U1$, V	U_{max}, V
1	203.53	3.18	71.06	214.09	0.66133	0.15258
2	204.71	2.75	74.88	224.55	0.67151	0.15247
3	212.94	2.66	74.68	225.24	0.67174	0.15103
4	211.77	2.68	74.60	224.84	0.67143	0.15042
5	210.59	2.73	74.28	223.81	0.67049	0.15055
				Maximum deviation	0.78%	0.71%

The results demonstrate that the maximum deviations of U_{max} do not exceed 0.28%. The maximum value of U_{max} for the ML with broad-side coupling covered by the ice layer was 0.2002 V, the water layer – 0.175 V and in the air filling – 0.1526 V. The resulting minimum and maximum U_{max} values for all cases considered were 0.1504 V and 0.2002 V, respectively. The minimum and maximum $U1$ values for all cases were 0.6717 V and 0.3235 V, respectively.

Finally, we performed a multicriteria optimization according to the matching and minimization criteria for the amplitude at the end of the turns. The ranges of variable geometric parameters and normalization coefficients were the same as in the optimization of these lines by the matching criterion. The optimization results are summarized in Tables 12–14. It can be seen that the maximum deviations of $U1$ and U_{max} values are within 0.18% and 0.89%, respectively. The obtained minimum and maximum U_{max} values for all cases were 0.1821 V and 0.2088 V, respectively. This difference is due to the inability to simultaneously provide a signal amplitude of 0.5 V at the beginning of the turn and a minimum amplitude at the output in the air filling. This can be explained by the narrow range of parameters to be changed and their small number. The minimum and maximum values of $U1$ were 0.499 V and 0.501 V, respectively. At the same time the obtained values of the parameters w and ε_r at each run are different.

TABLE 12. GA results for the ice-covered turn according to criteria (6) and (7).

Launch number	w, μm	ε_r	Z_o, Ω	Z_e, Ω	$U1$, V	U_{max}, V
1	430.59	4.80	23.85	123.22	0.499821	0.20836
2	377.65	5.86	24.15	121.42	0.499631	0.20878
3	582.35	2.80	23.47	126.27	0.500019	0.20857
4	301.18	7.88	24.92	118.20	0.499828	0.20779
5	349.41	6.47	24.47	120.55	0.500152	0.20792
				Maximum deviation	0.05%	0.24%

TABLE 13. GA results for the water-covered turn according to criteria (6) and (7).

Launch number	w, μm	ε_r	Z_o, Ω	Z_e, Ω	$U1$, V	U_{max}, V
1	93.14	2.59	30.03	96.48	0.49967	0.183385
2	95.10	2.33	29.99	96.30	0.49903	0.183155
3	93.53	2.47	30.04	96.49	0.49964	0.183617
4	94.31	2.28	30.06	96.46	0.49951	0.182128
5	93.14	2.38	30.10	96.62	0.49999	0.182635
				Maximum deviation	0.1%	0.41%

TABLE 14. GA results for the air-filled turn according to criteria (6) and (7).

Launch number	w, μm	ε_r	Z_o, Ω	Z_e, Ω	$U1$, V	U_{max}, V
1	509.41	5.39	33.59	119.19	0.4994	0.1902
2	581.57	4.8	32.75	121.58	0.501	0.1964
3	584.71	4.8	32.65	121.47	0.5006	0.1976
4	504.71	5.36	33.83	119.59	0.5004	0.1909
5	507.84	5.41	33.58	119.06	0.4992	0.1911
				Maximum deviation	0.18%	1.89%

To compare the results, we performed the optimization using ES according to the criterion of minimizing the amplitude at the turn output. The optimization results are summarized in Table 15.

TABLE 15. ES results for the turn covered with by ice, water, and in the air filling according to the amplitude minimization criterion.

Launch number	Ice layer			Water layer			Air filling		
	w, μm	ε_r	U_{max}, V	w, μm	ε_r	U_{max}, V	w, μm	ε_r	U_{max}, V
1	341.5	2.2	0.1998	411.19	3.02	0.1776	205.24	2.91	0.1511
2	302.37	2.67	0.2002	457.12	2.64	0.1779	208.22	2.92	0.1528
3	320.6	2.64	0.2006	405.86	2.84	0.1764	204.27	2.93	0.1517
4	303.72	2.9	0.2	407.06	2.98	0.1767	203.36	3.09	0.1522
5	304.62	2.96	0.2007	427.11	2.73	0.1768	200.48	3.14	0.1517
Maximum deviation			0.22%	–		0.44%	–		0.55%

The geometric parameters and ranges of the desired parameters were chosen the same as in the GA optimization. The number of calculations is assumed to be 100. Such number of calculations for the structure under investigation, when the variable parameters and their ranges are considered, provided the desired set of parameters and good convergence (the maximum deviation of U_{max} values did not exceed 0.55%). The average time for one run was about 90 s. This means that ES was faster than GA on average by 3.33 times in this example.

CONCLUSION

The paper, for the first time, has demonstrated the changes in the ML turn characteristics in the presence of water and ice. In addition, the possibility of using GA or ES together with a temperature model have been demonstrated for the parametric optimization of the ML turn, taking into account the influence of water and ice layers. During the analysis, we revealed the following:

- the presence of water and ice significantly influences the ML turn characteristics;
- the influence of the water and ice layers on each characteristic of the turn is different;
- the delays of the even and odd mode pulses (with respect to air filling) for the ice-covered turn increased by 39.3% and 12%, and for the water-covered turn – by 177.1% and 248%, respectively;

the maximum changes in τ_o, τ_e, Z_e, Z_o and U_{max} in their variable ranges differ in the three cases (water, ice and air filling).

The study shows that the temperature model can be used together with GA or ES to find a set of optimal geometrical parameters of the cross-section. It is demonstrated that with optimal geometrical parameters, the deviation of the obtained characteristics from the reference ones under the influence of water and ice changes, which is important for practical applications. Based on the results of GA optimization together with the temperature model, we obtained the sets of optimal geometric parameters for the ML turn. These sets provide the minimum amplitude at its output for all three cases of the turn (ice, water, and air filling). The maximum deviation of the characteristics during GA optimization (two criteria, 5 runs) was 0.18% for the line input amplitude and 1.89% for the output amplitude. According to the ES optimization results, we obtained the optimal geometrical parameters of the turn, which provide the minimum amplitude at its output under the influence of water and ice. The maximum deviation of the amplitude at the turn output (5 runs) was 0.55%. The results of optimization by the two methods showed good agreement, but at similar sets of optimal parameters, the ES optimization turned out to be 3.3 times faster.

ACKNOWLEDGMENTS

The research was supported by the Russian Science Foundation, Project 22-79-00103 (simulation) and the Ministry of Science and Higher Education of the Russian Federation, Project FEWM-2022-0001 (temperature model).

REFERENCES

1. Y. Zhang and P. E. Bagnoli, Microelectronics Journal, **45**(**8**), 1033-1052 (2014).
2. S. Zhan, M. H. Azarian and M. Pecht, IEEE Transactions on Device and Materials Reliability **8(2)**, 426-434 (2008).
3. H. Nishiyama, T. Okamoto, Y. Kim, D. Fujimoto, and Y. Hayashi, "Fundamental Study on Influence of Intentional Electromagnetic Interference on IC Communication," *12th International Workshop on the Electromagnetic Compatibility of Integrated Circuits (EMC Compo)*, (Haining, China, 2019) pp. 1–3.
4. C. Mojert, D. Nitsch, H. Friedhoff and J. Maack, "UWB and EMP susceptibility of microprocessors and networks," *Proc. 14th Int. Zürich Symp. Electromagn. Compat.* pp. 47-52 Feb. 20–22. (2001).
5. X. Yu, Z. Ma, C. Chai, C. Shi and P. Wang, IEEE Transactions on Electromagnetic Compatibility, **62(1)**, 101-107 (2020).
6. R. Krzikalla, T. Weber and J. L. ter Haseborg, IEEE International Symposium on Electromagnetic Compatibility, 1313-1316 (2003).
7. R. Krzikalla, J. L. ter Haseborg, International Symposium on Electromagnetic Compatibility, 977-981 (2005).
8. T. Weber, R. Krzikalla, JL ter Haseborg, IEEE Trans. on EMC, **36(3)**, 423-430 (2004).
9. Q. Cui, *et al*., "Investigation of waffle structure SCR for electrostatic discharge (ESD) protection," *in IEEE International Conference on Electron Devices and Solid-State* Circuit (EDSSC), (Bangkok, Thailand, Dec, 2012), pp. 3–5.
10. H. Hayashi, *et al*., "ESD protection design optimization using a mixed-mode simulation and its impact on ESD protection design of power bus line resistance," in *International Conference on Simulation of Semiconductor Processes and Devices, 2005* (SISPAD 2005), (Tokyo, Japan, 2005) pp. 99–102.
11. Z. M. Gizatullin and R. M. Gizatullin, Journal of Communications Technology and Electronics, **5**, 546–550 (2016).
12. S. A. Zajkova, *Passive components of electronic equipment* (Grodno: GrGU, 2009).
13. A. S. Koldunov, *Radio alphabet. Analog devices* (M: Solon-Press, 2004).
14. R. S. Surovtsev, T. R. Gazizov and A. M. Zabolotsky, International Siberian Conference on Control and Communications **2015**, 1-5.
15. A. V. Nosov, R. S. Surovtsev, International Multi-Conference on Engineering, Computer and Information Sciences **2017**, 453-458.
16. V. P. Kostelecky, A. M. Zabolotsky and A. M. Lakoza, Problems of developing advanced micro- and nanoelectronic systems **4**, 127-133 (2021).
17. M. A Samoilichenko and T. R Gazizov, MES **4**, 134-139 (2021).

18. K. P. Malygin, A. V. Nosov and R. S. Surovtsev, 2022 International Ural Conference on Electrical Power Engineering **2022**, 273-278 (2022).
19. S. P Kuksenko, IOP Conf. Series: Materials Science and Engineering **560**, 012110 (2019).
20. I. Y Sagiyeva, A. V. Nosov and R. S. Surovtsev, 21st International Conference of Young Specialists on Micro/Nanotechnologies and Electron Devices **2020**, 191-194.
21. G. S. Landsberg, *Elementary textbook of physics. mechanics. heat. Molecular physics* (M.: Nauka, 1985).
22. M. Nowottnick, Technology in the electronics industry, **8**. 51–55 (2009).
23. Li. Hua-Min, R. Chang-Ho, Z. Gang and Y. Won Jong, Journal of the Korean Physical Society, **2009**, 1096-1099.
24. A. O. Belousov, T. R. Gazizov, Complexity, **2018**.